



## Electroless Deposition of Silver on Multiwalled Carbon Nanotubes Using Iodide Bath

Susumu Arai<sup>\*,z</sup> and Junko Fujii

Department of Chemistry and Material Engineering, Faculty of Engineering, Shinshu University, Nagano 380-8553, Japan

Electroless deposition of silver on multiwalled carbon nanotubes (MWCNTs) was investigated using an iodide bath. Prior to electroless deposition of silver, the MWCNTs were chemically oxidized and then pre-treated using a typical two-step method (sensitization and activation) to form catalytic palladium nuclei on the MWCNTs. Dimethylaminoborane (DMAB) was used to reduce silver ions. Electroless deposition of silver was carried out at 25°C with variation of the pH. The microstructure of the deposits was evaluated using field emission-scanning electron microscopy (FE-SEM), X-ray diffraction (XRD), and transmission electron microscopy (TEM). The silver iodide complex ion species present was determined to be  $\text{AgI}_4^{3-}$  from equilibrium potential measurements. Silver was selectively deposited on palladium nuclei on the surface of the MWCNTs and continuous diffusion of deposited silver and palladium nuclei resulted in a solid solution of Ag-Pd alloy particles on the MWCNTs at pH = 7.5. © 2011 The Electrochemical Society. [DOI: 10.1149/1.3599066] All rights reserved.

Manuscript submitted April 19, 2011; revised manuscript received May 13, 2011. Published June 14, 2011

Carbon nanotubes (CNTs) (Refs. 1, 2) exhibit excellent mechanical characteristics, including high tensile strength and high elastic modulus, and have high thermal conductivity. CNTs are also expected to be applied as a superior support for catalytic nanoparticles due to their chemical and physical stability and large specific surface areas.

Silver nanoparticles have unique optical<sup>3-8</sup> and antibacterial properties,<sup>9-12</sup> and catalytic properties for glucose oxidation.<sup>13-15</sup> Among the fabrication methods employed to form silver nanoparticles on supports such as CNTs, electroless or chemical deposition methods are considered to be the most effective with respect to uniform distribution and minimized cost. The formation of silver nanoparticles on CNTs by electroless deposition has been reported,<sup>16,17</sup> in which ammonium baths that contain ammonia as the silver ion complexing agent are widely used.<sup>17-20</sup> However, fulminating silver compounds such as silver nitride ( $\text{AgN}_3$ ) and silver amide ( $\text{AgNH}_2$ ) may form in the ammonium baths. Iodides such as potassium iodide are known as a complexing agent for silver ions, and therefore silver electrodeposition baths using iodide have been investigated as non-cyanide baths.<sup>21-24</sup> However, electroless deposition of silver from an iodide bath has not been reported. The fabrication of silver nanoparticles on CNTs without the use of toxic or fulminating baths would be valuable not only for practical applications, but also from an academic perspective. Therefore, the electroless deposition of silver on CNTs was investigated using an iodide bath.

### Experimental

**Estimation of silver iodide complex ion species.**— Silver iodide complex ion species were estimated using equilibrium potential measurements. Equilibrium potentials were measured using an electrochemical measurement system (Hokuto Denko HZ-3000) at 25°C without agitation. AgI was dissolved in 1.5 M KI solution at various concentrations. Pure silver and platinum plates, and a saturated calomel electrode (SCE) were used as working, counter, and reference electrodes, respectively.

**Electroless silver deposition on CNTs.**— Commercially available vapor-grown multiwalled carbon nanotubes (MWCNTs: Showa Denko Co. Ltd., typically 80 nm diameter and 10–15  $\mu\text{m}$  long), formed via catalyst-assisted chemical vapor deposition and heat treated at 2800°C in argon for 30 min (graphitization) were used in the present study. The MWCNTs used in this study were graphitized MWCNTs; therefore, the surfaces of the MWCNTs were especially defect-free and chemically inert. Chemical oxidation is a useful method to enhance the chemical reactivity of MWCNTs surfaces.<sup>25-27</sup>

Therefore, prior to the electroless deposition process, the MWCNTs were refluxed in a mixture of acids ( $\text{HNO}_3:\text{H}_2\text{SO}_4 = 3:2$  v/v) for 12 h to oxidize the MWCNT surfaces, that is, to increase defects on the MWCNT surfaces. The oxidized MWCNTs were not dispersed homogeneously in the aqueous solutions, so that 0.05 g of oxidized MWCNTs was firstly dispersed in 0.05  $\text{dm}^3$  of a  $2 \times 10^{-5}$  M aqueous solution of polyacrylic acid (mean molecular weight is 5000: (PA-5000)) using stirrer agitation and ultrasonic irradiation. The PA-5000 dispersant was adsorbed on the MWCNTs and resulted in a homogeneous dispersion. After dispersion, the MWCNTs were filtrated and rinsed. The next pre-treatment of the MWCNTs before electroless deposition was carried out using a typical two-step method (sensitization and activation). The MWCNTs were immersed in a  $4.4 \times 10^{-2}$  M  $\text{SnCl}_2 \cdot 2\text{H}_2\text{O} + 0.12$  M HCl solution (0.1  $\text{dm}^3$ ) at 25°C with agitation (ultrasonic irradiation: 1 min, stirrer agitation: 5 min) to adsorb  $\text{Sn}^{2+}$  ions on the MWCNTs (sensitization). After filtration and rinsing, the MWCNTs were then immersed in a  $5.6 \times 10^{-4}$  M  $\text{PdCl}_2 + 0.12$  M HCl solution (0.1  $\text{dm}^3$ ) at 25°C with agitation (ultrasonic irradiation: 1 min, stirrer agitation: 5 min) to form catalytic palladium nuclei on the MWCNTs (activation). The pre-treated MWCNTs were then placed in a silver iodide complex bath (0.02 M AgI + 1.5 M KI solution: 0.45  $\text{dm}^3$ ) and dispersed by agitation. 0.05  $\text{dm}^3$  of 0.12 M dimethylaminoborane (DMAB) as a reducing agent for silver ions was then added to the AgI bath containing the MWCNTs at a rate of 0.01  $\text{dm}^3 \text{min}^{-1}$  at 25°C. Electroless deposition was continued for 5 min after complete addition of the reducing agent. The total volume of the solution was 0.5  $\text{dm}^3$  and the electroless deposition time was 10 min in total. The bath pH was varied from 7.5 to 13. After silver deposition, the MWCNTs were filtrated, rinsed, and dried. AgI is intrinsically a poorly water-soluble substance that does not dissolve in pure water. Consequently, the AgI remaining in the filtrate may deposit during rinsing with pure water. On the contrary, AgI is soluble in a high concentration iodide solution and forms complexes; therefore, the filtrated MWCNTs were firstly rinsed with 1 M KI solution and then rinsed with pure water.

**Characterization of the silver-deposited CNTs.**— The microstructures of the deposits were examined using field-emission scanning electron microscopy (FE-SEM; Jeol JSM-7000F), transmission electron microscopy (TEM; Jeol JSM-2100F), and X-ray diffraction (XRD; Shimadzu Seisakusho XRD-6000).

### Results and Discussion

Although AgI is intrinsically a poorly water-soluble species, it forms water-soluble iodide complex ions when plenty of iodide is present in the aqueous solution. The silver iodide complex ion species present in a 2 M AgI solution were estimated by Inoue et al. from equilibrium potential measurements.<sup>23</sup> The silver iodide

\* Electrochemical Society Active Member.

<sup>z</sup> E-mail: araisun@shinshu-u.ac.jp

complex ion species present vary according to the concentrations of KI and  $\text{Ag}^+$  ions. In the present study, a 1.5 M KI solution was used and the silver iodide complex ion species were estimated using the same method as Inoue et al.

The equilibrium of the  $\text{Ag}/\text{Ag}^+$  redox pair in aqueous solution is described as



The silver electrode potential  $E$ , is given by the Nernst equation

$$E = E^\circ + \frac{RT}{F} \ln a_{\text{Ag}^+} \quad [2]$$

where  $E^\circ$ ,  $R$ ,  $T$ ,  $F$ , and  $a_{\text{Ag}^+}$  are the standard electrode potential for the  $\text{Ag}/\text{Ag}^+$  redox pair, the gas constant, the absolute temperature, the Faraday constant, and the activity of silver ions, respectively.  $E^\circ(\text{Ag}/\text{Ag}^+) = 0.80$  V (Ref. 28) and  $T = 298$  K, so that Eq. 2 can be described using a decimal logarithm as follows

$$E = 0.80 + 0.059 \log a_{\text{Ag}^+} \quad [3]$$

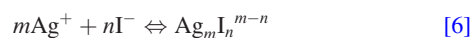
If  $a_{\text{Ag}^+}$  is approximated to the molality  $b_{\text{Ag}^+}$ , and furthermore approximated to the molar concentration  $[\text{Ag}^+]$ , then Eq. 3 can be described as follows

$$E = 0.80 + 0.059 \log [\text{Ag}^+] \quad [4]$$

In this study, the SCE was used as the reference electrode, and the difference between the standard hydrogen electrode (SHE) and the SCE is 0.241 V (+0.241 V vs. SHE at 25°C); therefore, the electrode potential vs. SCE is described as

$$E_{\text{SCE}} = 0.559 + 0.059 \log [\text{Ag}^+] \quad [5]$$

The equilibrium of complexation reactions of  $\text{Ag}^+$  ions in high concentration KI solution is described by the following general expression



In the present study, the concentration of iodide ions was 1.5 M. If the logarithm of the equilibrium constant for Eq. 6 is defined as a stability constant  $\beta_{nm}$ , then the stability constant can be described as

$$\beta_{nm} = \log \frac{[\text{Ag}_m\text{I}_n^{m-n}]}{[\text{Ag}^+]^m \cdot 1.5^n} \quad [7]$$

The total concentration of silver ions  $C_{\text{Ag}^+}$ , in the  $\text{AgI}$  solution is described as

$$C_{\text{Ag}^+} = [\text{Ag}^+] + [\text{Ag}_m\text{I}_n^{m-n}] \quad [8]$$

The values of  $\beta_{nm}$  are very large [see Eqs. 12–14]; therefore,  $[\text{Ag}^+]$  is considered to be much smaller than  $[\text{Ag}_m\text{I}_n^{m-n}]$ . Consequently,  $C_{\text{Ag}^+}$  is approximated as follows

$$C_{\text{Ag}^+} \approx [\text{Ag}_m\text{I}_n^{m-n}] \quad [9]$$

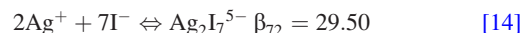
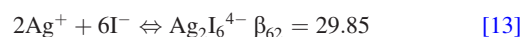
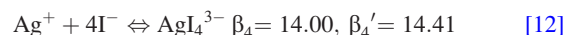
From Eqs. 7 and 9,  $[\text{Ag}^+]$  is described as

$$[\text{Ag}^+] = \left( \frac{C_{\text{Ag}^+}}{10^{\beta_{nm} \cdot 1.5^n}} \right)^{\frac{1}{m}} \quad [10]$$

Substituting Eq. 10 into Eq. 5 gives

$$E_{\text{SCE}} = 0.559 + \frac{0.059}{m} \log C_{\text{Ag}^+} - \frac{0.059}{m} (\beta_{nm} + \log 1.5^n) \quad [11]$$

Three silver iodide complex ions are mainly known, and their complexation reactions and corresponding  $\beta_{nm}$  are reported as<sup>29</sup>



Two stability constant values,  $\beta_4$  and  $\beta_4'$ , are reported by different researchers for the reaction of Eq. 12. Substituting the values for  $\beta_4$ ,  $\beta_4'$ ,  $\beta_{62}$ , and  $\beta_{72}$  into Eq. 11 gives the relational expressions between  $E_{\text{SCE}}$  and  $\log C_{\text{Ag}^+}$  for Eqs. 12, 13, and 14 as follows

$$E_{\text{SCE}}(\beta_4) = 0.059 \log C_{\text{Ag}^+} - 0.308 \quad [15]$$

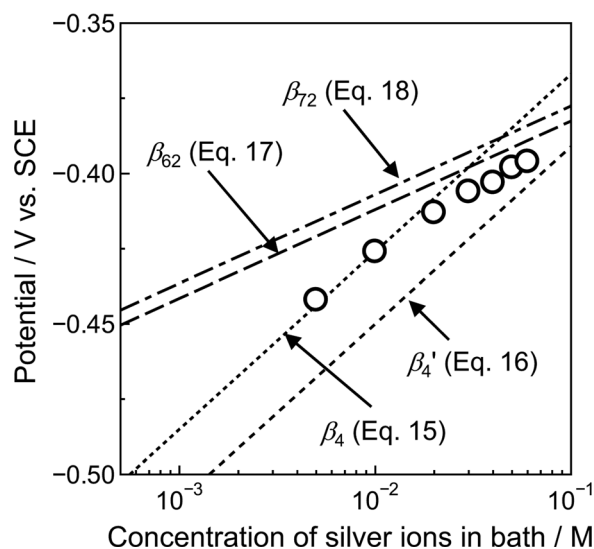
$$E_{\text{SCE}}(\beta_4') = 0.059 \log C_{\text{Ag}^+} - 0.332 \quad [16]$$

$$E_{\text{SCE}}(\beta_{62}) = 0.0295 \log C_{\text{Ag}^+} - 0.353 \quad [17]$$

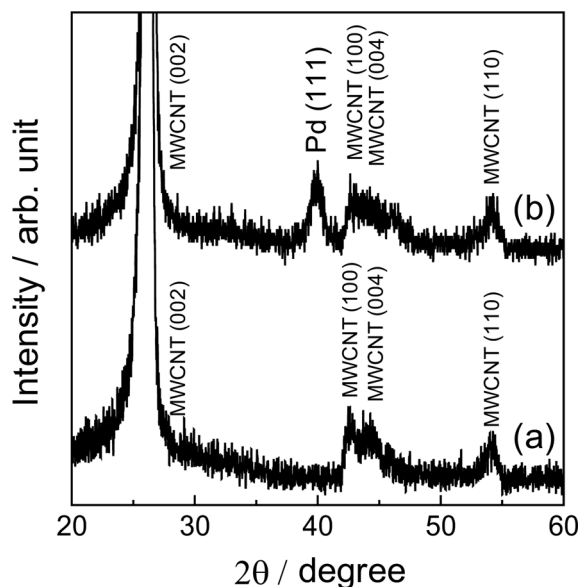
$$E_{\text{SCE}}(\beta_{72}) = 0.0295 \log C_{\text{Ag}^+} - 0.348 \quad [18]$$

Figure 1 shows the relationship between  $\log C_{\text{Ag}^+}$  and  $E_{\text{SCE}}$ . The circles indicate the electrode potentials measured against various  $C_{\text{Ag}^+}$ . The measured electrode potentials are proportional to  $\log C_{\text{Ag}^+}$  and correspond well with the line calculated using  $\beta_4 = 14.00$  in the  $C_{\text{Ag}^+}$  range below 0.02 M. Therefore, the silver iodide complex ion species could be estimated to be  $\text{AgI}_4^{3-}$ . Above  $C_{\text{Ag}^+} = 0.02$  M, the slope of the measured values decreases and becomes similar to the slope calculated using  $\beta_{62} = 29.85$  or  $\beta_{72} = 29.50$ . Inoue et al. reported that the silver iodide complex ion species were considered to change from  $\text{AgI}_4^{3-}$  ( $\beta_4 = 14.00$ ) to  $\text{Ag}_2\text{I}_6^{4-}$  ( $\beta_{62} = 29.85$ ) or  $\text{Ag}_2\text{I}_7^{5-}$  ( $\beta_{72} = 29.50$ ) above  $C_{\text{Ag}^+} = 0.03$  M in 2 M KI.<sup>23</sup> In the present study, the silver iodide complex ion species may change in a similar way. We also consider that the gap between the measured electrode potentials and the line calculated using  $\beta_4 = 14.00$  is due to the difference between  $a_{\text{Ag}^+}$  and  $[\text{Ag}^+]$ , because the mean activity coefficient generally decreases with increasing molar concentration. Regardless,  $[\text{Ag}^+]$  was 0.02 M in this study, so that the silver iodide complex ion species in the 1.5 M KI solution was estimated to be  $\text{AgI}_4^{3-}$ .

Figure 2 shows XRD patterns of the oxidized MWCNTs before and after the pre-treatment (sensitization and activation). Before pre-treatment, some peaks were assigned to the MWCNTs (Fig. 2a). In contrast, after pre-treatment, a peak assigned to face-centered-cubic palladium (111) plane is evident at 40°, in addition to the



**Figure 1.** Relationship between the concentration of silver ions in the bath and the rest potential. Measured values (circles) and estimated values calculated from stability constants of  $\beta_4 = 14.00$ ,  $\beta_4' = 14.41$ ,  $\beta_{62} = 29.85$ , and  $\beta_{72} = 29.50$ , are shown.

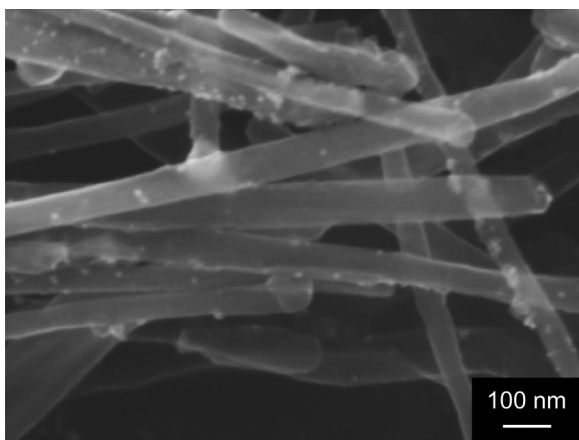


**Figure 2.** XRD patterns of MWCNTs (a) before and (b) after pre-treatment (sensitization and activation).

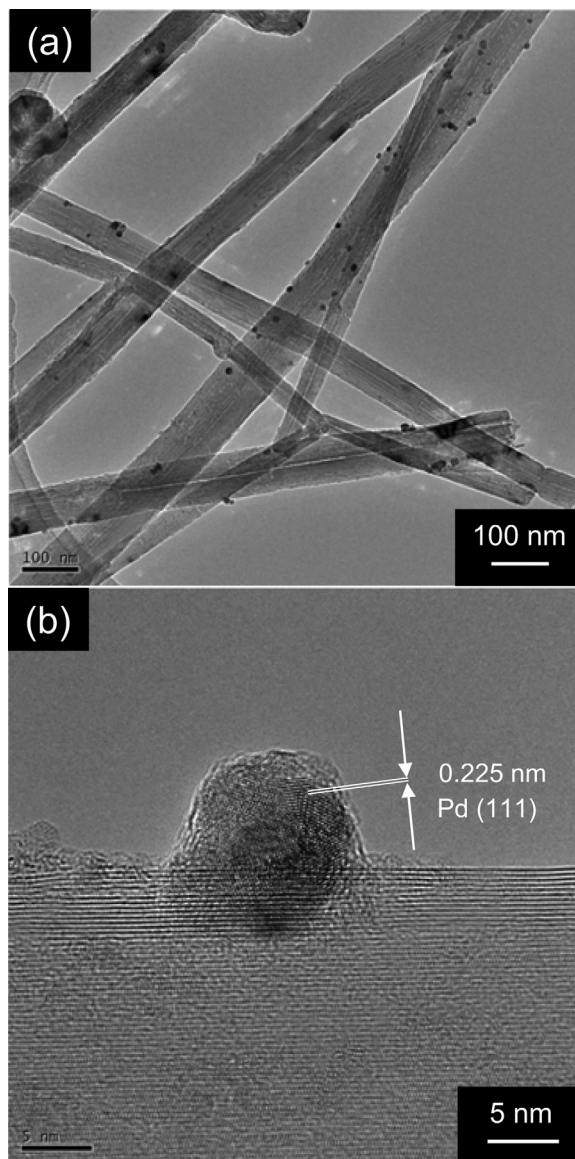
peaks assigned to the MWCNTs (Fig. 2b). Therefore, it is considered that palladium was deposited on the MWCNTs during the pre-treatment.

Figure 3 shows a SEM image of the MWCNTs after the pre-treatment, where small particles are present on the MWCNTs. These particles are considered to be the palladium particles, that is, palladium catalytic nuclei. Oxidation of the MWCNTs was conducted to introduce defects on the MWCNTs before the pre-treatment; therefore, it is considered that  $\text{Sn}^{2+}$  ions are selectively adsorbed on the defect sites during the sensitization step, and palladium particles are deposited on the same defect sites by a reductive process during the activation step.

Figure 4 shows TEM images of the MWCNTs after the pre-treatment. The black spots evident in Fig. 4a are palladium particles. The particles were several nanometers in size and their distribution was relatively uniform. A high-resolution TEM image indicated a lattice spacing of 0.225 nm for the palladium particles, which corresponds to the palladium (111) plane (Fig. 4b). It was also evident that some palladium particles were single crystals and some were polycrystalline, as shown by the high-resolution TEM image in Fig. 4b. Thus, the formation of face-centered-cubic palladium catalytic nuclei of several nanometers on the MWCNTs after the pre-treatment was confirmed.



**Figure 3.** SEM image of MWCNTs after pre-treatment (sensitization and activation).



**Figure 4.** (a) TEM image of MWCNTs after pre-treatment and (b) high-resolution TEM image of a Pd particle on a MWCNT.

Figure 5 shows XRD patterns of the MWCNTs after electroless silver deposition undertaken at various  $\text{pH}$  values. For comparison, XRD patterns of the MWCNTs before and after pre-treatment are also shown in Figs. 5a and 5b, respectively. In the case of  $\text{pH} = 7.5$  (Fig. 5c), a small peak was observed at around  $39.5^\circ$ , which is slightly lower than the peak assigned to the face-centered-cubic palladium (111) plane shown in Fig. 5b. Figure 6 shows a SEM image of the MWCNTs after electroless silver deposition at  $\text{pH} = 7.5$ , where small particles are apparent on the MWCNTs. Deposits were observed only on the MWCNTs. High-resolution TEM observation of the MWCNTs after electroless silver deposition at  $\text{pH} = 7.5$  (Fig. 7) indicated the size of the deposits was approximately 10–15 nm. A lattice spacing of the deposit was found to be 0.225 nm, which corresponds to the diffraction angle  $2\theta = 39.5^\circ$  according to Bragg's law

$$2d\sin\theta = n\lambda \quad [19]$$

where  $d$  is the lattice spacing,  $\theta$  is the Bragg angle,  $n$  is integer (in this case  $n = 1$ ), and  $\lambda$  is the wavelength of the X-rays ( $\lambda = 1.5405 \text{ \AA}$ ). The value of  $2\theta = 39.5^\circ$  is consistent with the diffraction angle

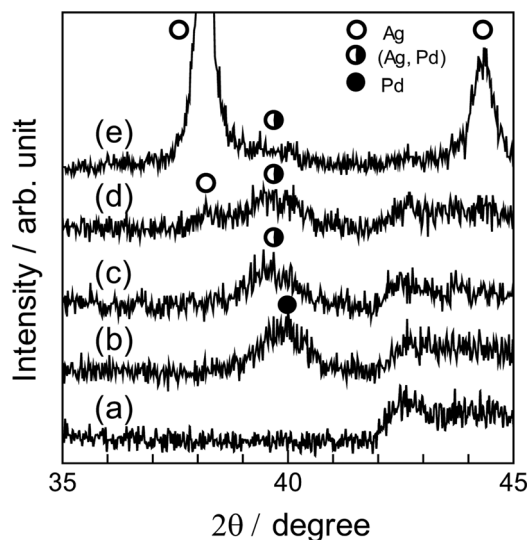
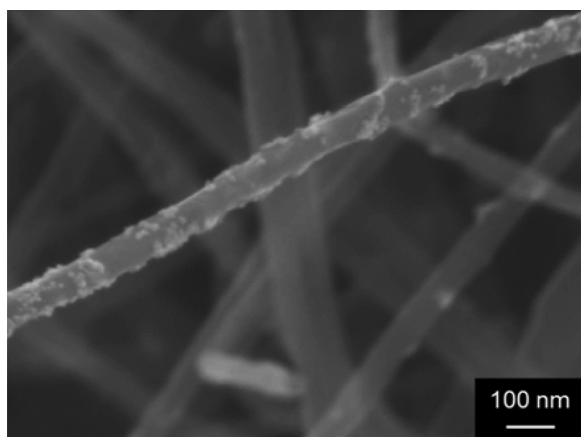


**Figure 5.** XRD patterns of MWCNTs after electroless silver deposition at various  $pH$ : (c)  $pH=7.5$ , (d)  $pH=10$ , and (e)  $pH=13$ . XRD patterns of MWCNTs (a) before and (b) after pre-treatment are also presented for comparison.

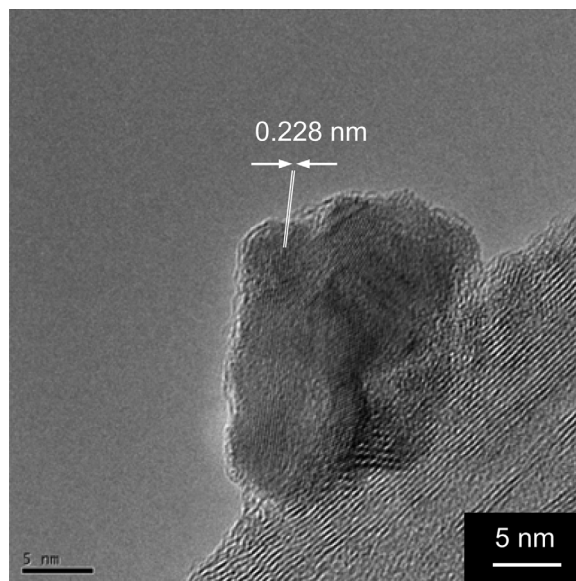
measured by XRD (Fig. 5c). The lattice spacings of the face-centered-cubic silver (111), (200), and (220) planes are 0.2359, 0.2044, and 0.1445 nm, respectively.<sup>30</sup> In contrast, those of the face-centered-cubic palladium (111), (200), and (220) planes are 0.2246, 0.1945, and 0.1376 nm, respectively.<sup>31</sup> The observed lattice spacing of 0.228 nm is between the lattice spacing of the silver (111) plane (0.2359 nm) and that of the palladium (111) plane (0.2246 nm).

Figure 8 shows the Ag-Pd alloy phase diagram,<sup>32</sup> where silver and palladium thermodynamically form solid solution alloys at all compositions. Therefore, it is considered that silver is deposited selectively on the palladium catalytic nuclei and continuously diffuses into the palladium particles, or counter diffusion between deposited silver particles and palladium particles occurs and results in the formation of a solid solution of Ag-Pd alloy particles on the MWCNTs. The sizes of the palladium particles and deposited silver were both very small (nanometer order); therefore, thermodynamically stable Ag-Pd alloy particles should be formed immediately.

The peak at around  $39.5^\circ$  in Fig. 5c may be assigned to the Ag-Pd solid solution. According to Vegard's Law, the lattice constant of a solid solution alloy varies in proportion to the composition. Therefore, the peak at around  $39.5^\circ$  can be assigned to the diffraction of the (111) plane of a face-centered-cubic Ag-Pd solid solution alloy. At  $pH=10$ , a weak peak was visible at around  $38^\circ$  in addition

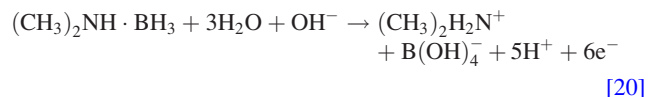


**Figure 6.** SEM image of MWCNTs after electroless silver deposition at  $pH=7.5$ .



**Figure 7.** High-resolution TEM image of a silver deposited on a MWCNT by electroless silver deposition at  $pH=7.5$ . This deposit was identified as a Ag-Pd alloy nanoparticle.

to the peak assigned to the Ag-Pd (111) plane (Fig. 5d). According to the Ag-Pd phase diagram (Fig. 8), there is only the stable Ag-Pd solid-solution alloy phase (Ag, Pd) at room temperature, so that the XRD peak at around  $38^\circ$  could be assigned to the face-centered-cubic silver (111) plane. SEM images (data not shown) of the MWCNTs after electroless silver deposition at  $pH=10$  indicated that the amount of deposit increased compared to that for deposition at  $pH=7.5$ . Sverdllov et al. reported that the anodic reaction of the DMAB reducing agent on the catalytic surface in alkaline solution could be described as follows<sup>33</sup>



According to Eq. 20, the oxidation reaction of DMAB is accelerated with increasing  $pH$  value by Le Chatelier's principle. The  $pH$  of the AgI solution in the present study was more than 7.5, so that the

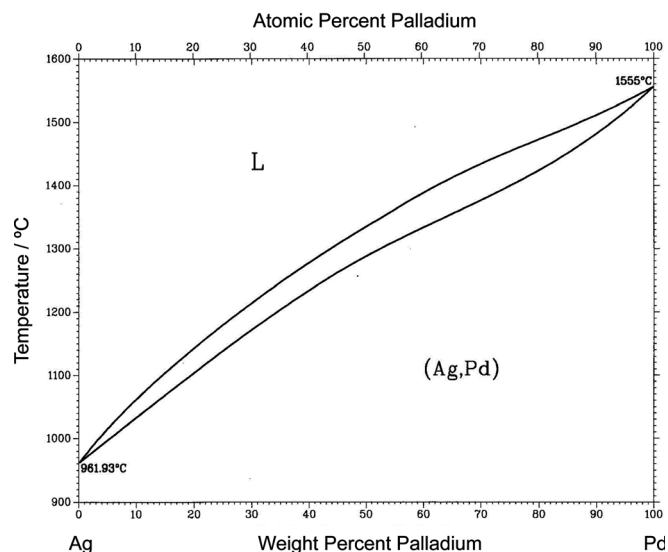


**Figure 8.** Ag-Pd binary alloy phase diagram.<sup>32</sup>

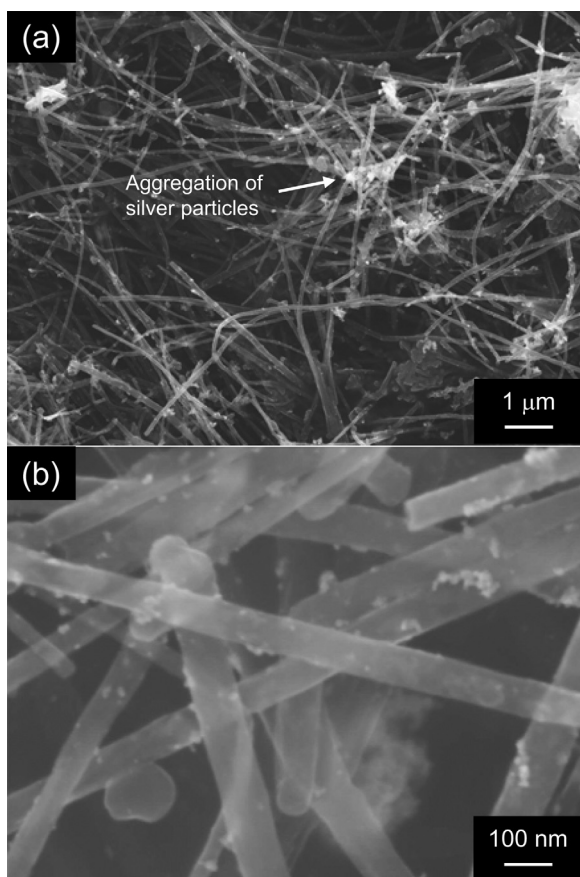
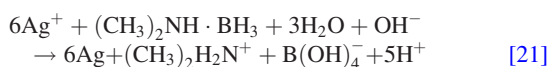


**Figure 9.** SEM images of MWCNTs after electroless silver deposition at  $pH = 13$ ; (a) low and (b) high magnification.

anodic reaction of DMAB should proceed according to Eq. 20 during electroless silver deposition. Therefore, the electroless deposition rate of silver would increase with increasing  $pH$ , which would result in a large amount of silver deposition on palladium nuclei at  $pH = 10$  compared to that at  $pH = 7.5$ . Consequently, silver particles that had not completely diffused into the palladium nuclei would remain on the palladium nuclei at  $pH = 10$ . Furthermore, it is considered that silver particles are not only deposited on the palladium catalytic nuclei, but also directly on the surface of the MWCNTs at  $pH = 10$ . At  $pH = 13$ , strong XRD peaks were observed at  $38^\circ$  and  $44.3^\circ$  (Fig. 5e), in addition to the peak assigned to the Ag-Pd (111) plane. Figure 9 shows SEM images of the MWCNTs after electroless silver deposition at  $pH = 13$ . Many particles were observed on the MWCNTs (Fig. 9b); however, some aggregates of particles were also evident among the silver-deposited MWCNTs (Fig. 9a). It is considered that silver is deposited not only on the palladium nuclei on the surface of the MWCNTs and on the surface of the MWCNTs, but also in the AgI bath, due to the highly reductive effect of DMAB at  $pH = 13$ , which results in the formation of silver particle aggregates. In other words, degradation of the AgI bath occurred. Therefore, the diffraction peaks at  $38$  and  $44.3^\circ$  in Fig. 5e could be assigned to the face-centered-cubic silver (111) and (200) planes, respectively. The diffraction peaks may be mainly due to silver particle aggregates; however, degradation of the AgI bath did occur and silver was not deposited selectively and homogeneously on the MWCNTs at  $pH = 13$ .

From Eqs. 1 and 20, the overall redox reaction during electroless silver deposition could be described as follows



Silver is deposited onto palladium catalytic nuclei on MWCNTs selectively and diffuses into the palladium catalytic nuclei, which results in the formation of nanoparticles on the MWCNTs at  $pH = 7.5$  that consist of a Ag-Pd solid solution alloy.

## Conclusions

Electroless silver deposition on pre-treated MWCNTs was performed using an iodide bath with DMAB as a reducing agent at various  $pH$  to form silver nanoparticles on MWCNTs. The silver iodide complex ion species was determined to be  $\text{AgI}_4^{3-}$  according to equilibrium potential measurements. Silver was selectively deposited onto palladium catalytic nuclei on the MWCNTs and continuously diffused into the palladium nuclei, which resulted in the formation of Ag-Pd alloy nanoparticles on the MWCNTs at  $pH = 7.5$ . Future work will include investigation of the catalytic properties of MWCNTs loaded with Ag-Pd alloy nanoparticles.

## Acknowledgments

This research was supported by Program for Fostering Regional Innovation in Nagano, granted by MEXT, Japan. The authors thank Prof. H. Muramatsu of the Institute of Carbon Science and Technology for conducting the TEM observations.

## References

1. A. Oberlin, M. Endo, and T. Koyama, *J. Cryst. Growth*, **32**, 335 (1976).
2. S. Iijima, *Nature* (London), **354**, 56 (1991).
3. W. Gotschy, K. Vonmetz, A. Leitner, and F. R. Aussenegg, *Opt. Lett.*, **21**, 1099 (1996).
4. H. Inoue, K. Tanaka, I. Tanahashi, T. Hattori, and H. Nakatsuma, *Jpn. J. Appl. Phys.*, **39**, 5132 (2000).
5. Y. Gao, Y. Wang, Y. Song, Y. Li, S. Qu, H. Liu, B. Dong, and J. Zu, *Opt. Commun.*, **223**, 103 (2003).
6. S. Porel, S. Singh, S. S. Harsha, D. N. Rao, and T. P. Radhakrishnan, *Chem. Mater.*, **17**, 9 (2005).
7. B. H. Choi, H. H. Lee, S. Jin, S. Chun, and S. H. Kim, *Nanotechnology*, **18**, 075706 (2007).
8. S. Camelio, D. Babonneau, D. Lantiat, L. Simonot, and F. Pailloux, *Phys. Rev. B*, **80**, 155434 (2009).
9. L. Zhang, J. C. Yu, H. Y. Yip, Q. Li, K. W. Kwong, A. W. Xu, and P. K. Wong, *Langmuir*, **19**, 10372 (2003).
10. J. R. Morones, J. L. Elechiguerra, A. Camacho, K. Holt, J. B. Kouri, J. T. Ramirez, and M. J. Yacamán, *Nanotechnology*, **16**, 2346 (2005).
11. P. Jain and T. Pradeep, *Biotechnol. Bioeng.*, **90**, 59 (2005).
12. S. Pal, Y. K. Tak, and J. M. Song, *Appl. Environ. Microbiol.*, **73**, 1712 (2007).
13. M. Tominaga, T. Shimazoe, M. Nagashima, H. Kusuda, A. Kubo, Y. Kuwahara, and I. Taniguchi, *J. Electroanal. Chem.*, **590**, 37 (2006).
14. J. Lin, C. He, Y. Zhao, and S. Zhang, *Sens. Actuators B*, **137**, 768 (2009).
15. H. Quan, S. U. Park, and J. Park, *Electrochim. Acta*, **55**, 2232 (2010).
16. W. T. Ebbesen, H. Hiura, M. E. Bisher, M. M. J. Treacy, J. L. Shreeve-Keyer, and R. C. Haushalter, *Adv. Mater.*, **8**, 155 (1996).
17. Y. Oh, D. Suh, Y. Kim, E. Lee, J. S. Mok, J. Choi, and S. Baik, *Nanotechnology*, **19**, 495602 (2008).
18. S. G. Warrier and R. Y. Lin, *J. Mater. Sci.*, **28**, 4868 (1993).
19. J. Jang and S. K. Ryu, *J. Mater. Process. Technol.*, **180**, 66 (2006).
20. J. Liu, B. Huang, X. Li, P. Li, and X. Zeng, *J. Electron. Mater.*, **39**, 2702 (2010).
21. K. P. Batashev and B. G. Kitaichik, *Tsvetnykh Metal*, **188**, 239 (1957).
22. H. Inoue, K. Yamakawa, T. Kondo, and S. Masaki, *J. Surf. Finish. Soc. Jpn.*, **41**, 1178 (1990).
23. H. Inoue, K. Yamakawa, and S. Masaki, *J. Surf. Finish. Soc. Jpn.*, **44**, 55 (1993).
24. O. A. Ashiru, *Plat. Surf. Finish.*, **82**, 76 (1995).
25. H. Hiura, T. W. Ebbesen, and K. Tanigaki, *Adv. Mater.*, **7**, 275 (1995).
26. B. Kim and W. M. Sigmund, *Langmuir*, **20**, 8239 (2004).
27. V. Datsyuk, M. Kalyva, K. Papangelis, J. Parthenios, D. Tasis, A. Siokou, I. Kallitisis, and C. Galiotis, *Carbon*, **46**, 833 (2008).
28. P. Atkins and J. D. Paula, *Atkins' Physical Chemistry*, 9th ed., p. 929, Oxford University, Oxford (2010).
29. J. Bjerrum, G. Schwarzenbach, and L. G. Sillen, *Stability Constants, Part II Inorganic Ligands*, p. 119, The Chemical Society, London (1958).
30. JCPDS Card: 00-004-0783.
31. JCPDS Card: 00-005-0681.
32. The Materials Information Society, *Binary Alloy Phase Diagrams*, 2nd ed., ASM International, Materials Park, OH (1996).
33. Y. Sverdlov, V. Bogush, H. Einati, and Y. Shacham-Diamand, *J. Electrochem. Soc.*, **152**, C631 (2005).